

Original Research

In Silico Insight to Identify Potential Inhibitors of BUB1B from Mushroom Bioactive Compounds to Prevent Breast Cancer Metastasis

Divya Mishra^{1,†}, Ashish Mishra^{1,†}, Sachchida nand Rai², Santosh kumar Singh², Emanuel Vamanu^{3,*}, Mohan P. Singh^{4,*}¹Centre of Bioinformatics, University of Allahabad, 211002 Prayagraj, Uttar Pradesh, India²Centre of Experimental Medicine and Surgery, Institute of Medical Sciences, Banaras Hindu University, 221005 Varanasi, Uttar Pradesh, India³Faculty of Biotechnology, University of Agricultural Sciences and Veterinary Medicine, 011464 Bucharest, Romania⁴Centre of Biotechnology, University of Allahabad, 211002 Prayagraj, Uttar Pradesh, India*Correspondence: email@emanualvamanu.ro (Emanuel Vamanu); mpsingh.16@gmail.com (M.P. Singh)

†These authors contributed equally.

Academic Editor: Amedeo Amedei

Submitted: 21 February 2023 Revised: 2 May 2023 Accepted: 8 June 2023 Published: 27 July 2023

Abstract

Background: Breast cancer is one of the most common types of cancer among women worldwide, and its metastasis is a significant cause of mortality. Therefore, identifying potential inhibitors of proteins involved in breast cancer metastasis is crucial for developing effective therapies. BUB1 mitotic checkpoint serine/threonine kinase B (BUB1B) is a key regulator of mitotic checkpoint control, which ensures the proper segregation of chromosomes during cell division. Dysregulation of BUB1B has been linked to a variety of human diseases, including breast cancer. Overexpression of BUB1B has been observed in various cancer types, and its inhibition has been shown to induce cancer cell death. Additionally, BUB1B inhibition has been suggested as a potential strategy for overcoming resistance to chemotherapy and radiation therapy. Given the importance of BUB1B in regulating cell division and its potential as a therapeutic target, the development of BUB1B inhibitors has been the focus of intense research efforts. Despite these efforts, few small molecule inhibitors of BUB1B have been identified, highlighting the need for further research in this area. In this study, the authors aimed to identify potential inhibitors of BUB1B from mushroom bioactive compounds using computational methods, which could ultimately lead to the development of new treatments for breast cancer metastasis. **Methods:** This study has incorporated 70 bioactive compounds (handpicked through literature mining) of distinct mushrooms that were considered and explored to identify a suitable drug candidate. Their absorption, distribution, metabolism and excretion (ADME) properties were obtained to predict the drug-likeness of these 70 mushroom compounds based on Lipinski's rule of 5 (RO5). Screening these bioactive compounds and subsequent molecular docking against BUB1B provided compounds with the best conformation-based binding affinity. The best two complexes, i.e., BUB1B-lepitaprocerin D and BUB1B-peptidoglycan, were subjected to molecular dynamic simulations. Both complexes were assessed for their affinity, stability, and flexibility in protein-ligand complex systems. **Results:** The molecular dynamic (MD) simulation studies revealed that lepitaprocerin D has an energetically favorable binding affinity with BUB1B. Results showed that the formation of a hydrogen bond between residues ASN123 and SER157, and lepitaprocerin D had strengthened the affinity of lepitaprocerin D with BUB1B. **Conclusions:** This study identified lepitaprocerin D as a potential and novel inhibitor for BUB1B that could be a plausible drug candidate for identifying and controlling the spread of breast cancer metastasis.

Keywords: lepitaprocerin D; molecular docking; molecular dynamics simulation; BUB1B; ADMET; aneuploidy; tumorigenesis

1. Introduction

The spindle assembly checkpoint (SAC) is deployed by cells during mitosis to prevent segregation errors resulting from unattached or improperly attached chromosomes [1]. The SAC remains active at the kinetochore until it becomes stably attached to the spindle apparatus. Ultimately, SAC satisfaction leads to the release of cell division cycle protein 20 (CDC20) from the inhibitory mitotic checkpoint complex allowing activation of the anaphase-promoting complex, or cyclosome (APC/C) [2]. Once activated by CDC20, the APC/C E3 ubiquitin ligase targets several proteins for degradation, including securin, ultimately leading to sister chromatid separation and triggering

anaphase onset. SAC activity at the kinetochore is orchestrated by a network of protein interactions and the activity of several protein kinases, including Mucopolysaccharidosis Type-1 (MPS1), Aurora B, and *BUB1*. MPS1 phosphorylation of Mellitin (MELT) recruits the knl1 kinetochore protein and enables SAC activation by recruiting other SAC proteins, such as Bub1 [2]. Aurora B is localized to centromeres via a combination of Haspin-mediated phosphorylation of histone H3 (H3pT3) and Bub1-mediated phosphorylation of histone H2A at Thr120 (H2ApT120), where it is required to promote correct kinetochore attachment and regulate the SAC.



Similar to Aurora B, Bub1 has been described as having a dual role in the SAC and chromosome alignment. While its contribution to chromosome alignment has been consistently demonstrated, studies have yielded conflicting results regarding the requirement of Bub1 for the SAC [3]. Generation of conditional knockout mouse embryonic fibroblasts (MEFs) and RNA interference (RNAi) knockdown from Henrietta Lacks (HeLa) and Human retinal pigment epithelial-1 (RPE1) cells found Bub1 to be essential for the SAC. Conversely, initial clustered regularly interspaced short palindromic repeats and CRISPR-associated protein 9 (CRISPR-CAS9) genome editing approaches in RPE1 and near-haploid human cell line (HAP1) cells suggested only a minor role for Bub1 in the SAC when cells were sensitized via Mps1 inhibition. These conflicting results were initially reconciled by the discovery that nonsense-associated alternative splicing allows for Bub1 expression following CRISPR-CAS9. The short interfering RNA (siRNA) knockdown of residual *BUB1* significantly impaired SAC response in *BUB1*-disrupted cells. However, more recently, HAP1 cells with several *BUB1* exons absent from genomic DNA were created following the use of two guide RNAs for CRISPR-CAS9 [4]. Surprisingly, the SAC remained functional in these cells, even when the more extensive approach was combined with Bub1 siRNA knockdown [4]. However, the generation of a complete *BUB1* deletion was only possible in haploid HAP1 cells but not in several other cell lines.

Despite the controversy, these experimental systems have allowed functional evaluation of *BUB1*. *BUB1* has a Bub3-binding domain through which *BUB1* is localized to kinetochores [5]. The *BUB1* central region acts as a scaffold for *BUB1*-mediated localization of the Rod-Zw10-Zwilch (RZZ) complex, mitotic arrest deficiency 1/2 (Mad1/2), and CDC20 localization to kinetochores, and is required for the SAC function of *BUB1*. Numerous reports have found *BUB1* kinase activity dispensable for SAC activation; however, others suggest that Bub1-mediated phosphorylation of CDC20 may directly contribute to APC/C inhibition [6]. Similarly, there are conflicting reports on whether Bub1 kinase activity is required for chromosome alignment. Bub1 H2ApT120 phosphorylation localizes Shugoshin 1/2 (Sgo1/2) and Aurora B, and other proteins of the chromosome passenger complex (CPC), to centromeres and may integrate correction of attachment errors with SAC signaling [7–9]. Histone H2A threonine 120 phosphorylation (H2ApT120) is required to maintain centromeric Aurora B and SAC activity in the absence of histone H3 at threonine 3 (H3pT3). Finally, Bub1 is also autophosphorylated, both within the kinase domain activation segment and outside of this segment, which may have a role in regulating Bub1 localization [8].

Functional characterization of Bub1 would benefit from small-molecule kinase inhibitors. Drugs targeting Mps1 and Aurora B have been powerful tools for decipher-

ing kinase function and dissection of mitosis. A potent, specific Bub1 kinase inhibitor is of particular value since complete penetrance of genetic deletions or siRNA has been difficult in human cells, and only 4% of residual Bub1 is needed for SAC activity [10]. However, considering multiple conflicting reports regarding the function of Bub1, it is important that the inhibitors used to evaluate its function are properly validated [11]. Availability of potential drugs against BUB1 mitotic checkpoint serine/threonine kinase B (BUB1B) can help to suppress the possibilities of cancer and its metastasis. Thus, it is necessary to screen for the identification of potential molecules which can bind BUB1B and inhibit its activities [12–14].

Using natural compounds as the drug is always beneficial and preferable as they are comparatively safer in terms of their pharmacokinetics and dynamics. Studies reported that various edible mushrooms had considerable anticancer properties [15]. Over the last two decades, various reports have shown the antitumor properties of these edible mushrooms, which are most remarkable and seek the scientific community's attention worldwide [1,16]. These edible mushroom extracts' cost-effectiveness, natural occurrence, and negligible side effects make them favorable for medicinal use. *Pleurotus ostreatus* is one of the most cultivated and widely used edible mushrooms [17–19] which has various medicinal properties that include antitumor [8], antiatherogenic, antioxidative, and hypocholesterolemic activities [2,3]. Earlier in 2008, Jedinak *et al.* [14] reported that *P. ostreatus* possesses an inhibitory effect on human breast and colon cancer [10]; later, *P. ostreatus* extract was also explored for its anticancer effects on other cancers and found to be potent against erythroleukemia [6,20], and human gastric cancer [5,7,18]. Over the last decade, various structure-based *in silico* approaches, i.e., homology modeling, molecular docking, and MD simulation, are already in practice as a potential tool to screen compounds against a receptor protein with substantial accuracy [11,12]. As the 3-D structure of BUB1B (Protein Data Bank (PDB): 2WVI) is available (Fig. 1), it creates opportunities to perform structure-based studies for its molecular interaction. 2WVI has a theoretical weight of 20.06 kDa and is monomeric in nature, having Thr85, Tyr81, Gln58, Asp79, Tyr89, Ser96, Ser157, Tyr139, and Glu161 amino acid residues with a N-terminal domain [21]. The current study aims to screen bioactive compounds from a distinct variety of mushrooms to find potential lead compounds against the BUB1B target. For this purpose, 70 already reported bioactive compounds of mushrooms with anticancer properties were utilized. All 70 compounds were screened for their pharmacokinetics absorption, distribution, metabolism, and excretion (ADMET) properties. Suitable compounds were screened against BUB1B through a structure-based molecular interaction approach, i.e., molecular docking, and further, their stability and affinity were determined via molecular dynamic (MD) simulation.

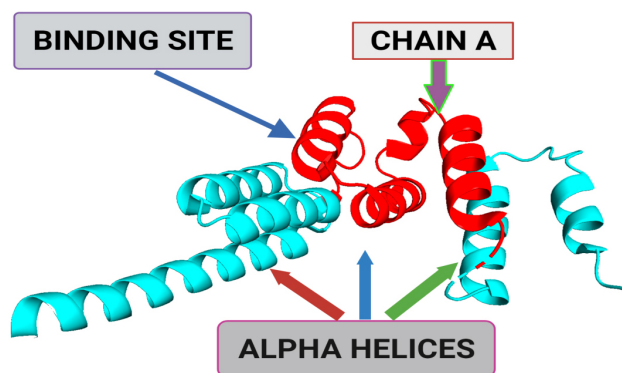


Fig. 1. A 3-dimensional structural representation of BUB1 mitotic checkpoint serine/threonine kinase B (BUB1B) (Protein Data Bank (PDB) ID: 2WVI; Resolution = 1.80 Å). The binding site represents the small pocket of 2WVI where ligands bind with the help of weak forces, i.e., non-covalent bonding. Chain A of 2WVI has a sequence length of 164. Alpha-helices are the spiral section of the secondary structure of the 2WVI protein, indicating the spatial arrangement of the main chain of 2WVI.

2. Materials and Methods

2.1 Screening and Selection of Mushroom Bioactive Compounds

The 70 bioactive compounds from edible mushrooms were obtained from literature mining. The essential predicted physicochemical descriptors of the selected compounds were obtained by calculating ADMET properties from SwissADME and helped screen compounds with favorable pharmacokinetic properties. A comprehensive analysis of the log P (octanol/water) and QP % (human oral absorption) was obtained from this SwissADME program. Another important element essential for rational drug design is Lipinski's rule of 5 (RO5) for bioactive compounds, which was also obtained from SwissADME and evaluated the acceptability of the known compounds.

2.2 Molecular Interaction Analysis through Docking

For screening of selected bioactive compounds against BUB1B (PDB: 2WVI), AutoDock Vina [22] was employed. Amongst these bioactive compounds with favorable pharmacokinetic properties, the top five compounds with optimal binding affinity scores were further filtered out, and these were then docked against the BUB1B receptor using AutoDock Vina. PyMol (v 2.5) was used to obtain the active site coordinates and residues of the receptor. This process was based on the pdb file of the receptor-ligand complex. PyMol provided the coordinates ($x_{center} = 0.4537$, $y_{center} = -24.6765$, $z_{center} = -12.2435$, $x_{size} = 60$, $y_{size} = 50$, $z_{size} = 70$) to obtain the grid parameter file, and these coordinates belong to chain-A of the protein; 72–165 residues. During the next step, the grid map files were obtained by running AutoGrid. These grid map files were then used for docking using AutoDock, v4.2.6 suite (The

Scripps Research Institute, Prayagraj, Uttar Pradesh, India) [23]. There were several standard parameters set for the docking purpose. These included hybrid Genetic Algorithm with Local Search (GA-LS) runs = 50, number of individuals in the population = 300, rate of gene mutation = 0.02, the maximum number of generations = 27,000, maximum number of energy evaluations = 2,500,000, and rate of crossover = 0.8. The algorithm employed for the AutoDock run was Lamarckian Genetic Algorithm (LGA), which provided RMSD (root-mean-square deviation) values and binding energies. Out of the five compounds, the top two with the best docking score were chosen for further validation using molecular dynamic simulation.

2.3 Molecular Dynamic Simulation

Desmond v3.6 Package [22] was employed for validating the findings of molecular docking using molecular dynamic simulation. This was performed to elucidate the effectiveness of these mushroom bioactive compounds for the activation of BUB1B. For this purpose, the preparation of the lead compounds viz. lepitaprocerin D and peptidoglycan (muramic acid) with BUB1B protein was completed using the optimized potentials for liquid simulations 2005 (OPLS2005) force field. To build the system, the predefined transferable intermolecular potential 3P (TIP3P) water model was used, and these acted as water molecules. The orthorhombic periodic conditions set at 10 Å units were used for constructing these. Before MD simulations, the energy minimization of the system was performed using the steepest-descent method, an optimization algorithm used to find the minimum energy state of a system by iteratively stepping in the direction of the steepest decrease in energy. Also, the balancing of Na^+/Cl^- was obtained to neutralize the charges of the complexes electrically. The steepest descent method was used as part of the complexes' minimization protocol; This helps reach a local minimum energy state, which can be used as a starting point for further simulations. The heating process was carried out at 0–300 K, having time steps of 0.001 ps and annealing steps of 2000. The system further normalized at 1000 steps in an equilibrium state with 0.001 ps time steps. The last step was the final production of the system that continued up to 100 ns at 300 K temperature and 1 Atm pressure at 0.001 ps time steps. These were applied by employing the Nose–Hoover method with NPT ensemble. The pictorial representation of the methodology employed for the present study is shown in Fig. 2.

3. Results

3.1 Absorption Distribution Metabolism Excretion Property Analysis

The 70 bioactive compounds obtained from different mushroom sources have been tabulated in Table 1 (Ref. [23–26]).

Table 1. List of 70 bioactive compounds obtained from mushrooms sources.

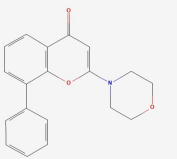
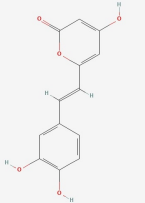
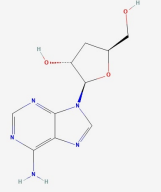
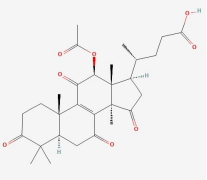
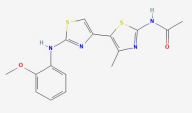
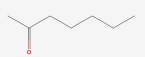
S.No.	Compound	Source	Structure	Reference
1	LY-294002	<i>Tricholoma matsutake</i>		[23]
2	Hispidine	<i>Phellinus linteus</i>		[23]
3	Cordycepin	<i>Cordyceps melitaris</i>		[23]
4	Lucidenic acid	<i>Ganoderma lucidium</i>		[23]
5	JNJ0966	<i>Hericium erinaceus</i>		[23]
6	2-Heptanone	<i>Hericium erinaceus</i>		[23]
7	Cyclobutanone	<i>Hericium erinaceus</i>		[23]
8	Cyclopropane	<i>Hericium erinaceus</i>		[23]

Table 1. Continued.

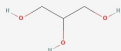
S.No.	Compound	Source	Structure	Reference
9	2(5H)-Furanone	<i>Hericium erinaceus</i>		[23]
10	Formamide	<i>Hericium erinaceus</i>		[23]
11	Glycerin	<i>Pleurotus ostreatus</i>		[23]
12	4-Heptanone	<i>Pleurotus ostreatus</i>		[23]
13	Propanedioic acid	<i>Pleurotus ostreatus</i>		[23]
14	Niacin	<i>Pleurotus ostreatus</i>		[23]
15	1,4-Pentanediol	<i>Pleurotus ostreatus</i>		[23]
16	3-Methyl-2-Pyrrolidinone	<i>Pleurotus ostreatus</i>		[23]

Table 1. Continued.

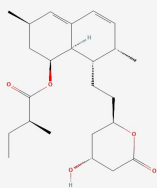
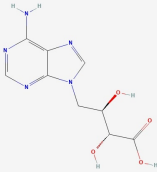
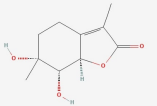
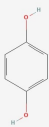
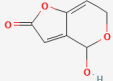
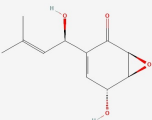
S.No.	Compound	Source	Structure	Reference
17	5-Methoxypyrrolidin-2-one	<i>Pleurotus ostreatus</i>		[23]
18	2-Undecene	<i>Pleurotus ostreatus</i>		[23]
19	Lovastatin	<i>Pleurotus ostreatus</i>		[23]
20	Eritadenine	<i>Lentinus edodes</i>		[23]
21	1,2-dihydroxymint Lactone	<i>Lentinus squarrosulus</i>		[23]
22	Hydroquinone	<i>Piptoporus betulinus</i>		[23]
23	Calvacin	<i>Calvatia gigantean</i>		[23]
24	Panepoxydone	<i>Lentinus crinitus</i>		[23]

Table 1. Continued.

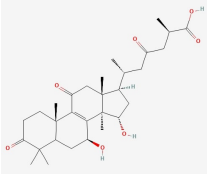
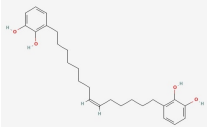
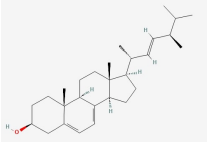
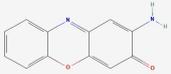
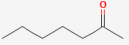
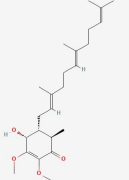
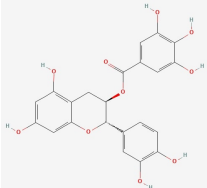
S.No.	Compound	Source	Structure	Reference
25	Gliotoxin	<i>Gliocladium fibriatum</i>		[23]
26	Ganoderic Acid	<i>Ganoderma lucidium</i>		[23]
27	Gerronemin D	<i>Gerronema sp.</i>		[23]
28	Ergosterol	<i>Grifola frondosa</i>		[23]
29	2-Amino-3H-Phenoxazin-3-one	<i>Lepiota Americana</i>		[23]
30	2_Heptanone	<i>Volvariella volvacea</i>		[23]
31	Antroquinonol	<i>Antrodia Camphorate</i>		[24]
32	(-)-Catechin	<i>Russula luteotacta</i>		[24]

Table 1. Continued.

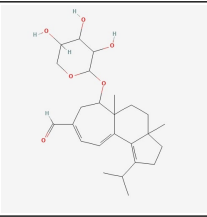
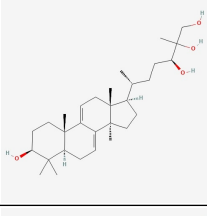
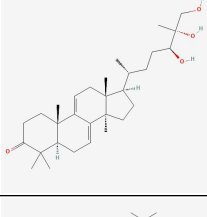
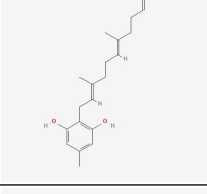
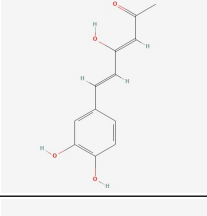
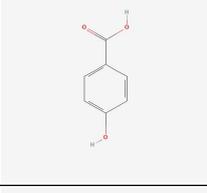
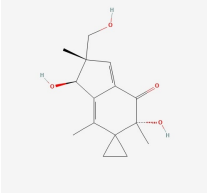
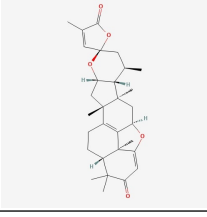
S.No.	Compound	Source	Structure	Reference
33	Erinacin A	<i>Hericium erinaceus</i>		[24]
34	Ganoderiol	<i>Ganoderma lingzhi</i>		[24]
35	Ganodermanontriol	<i>Ganoderma leucocontextum</i>		[24]
36	Grifolin	<i>Albatrellus confluens</i>		[24]
37	Hispolon	<i>Phellinus linteus</i>		[24]
38	4-Hydroxybenzoic Acid	<i>Rusulla emetic</i>		[24]
39	Illudin-S	<i>Omphalotus illudens</i>		[24]
40	Lepiotaprocerin C	<i>Macrolepiota procera</i>		[24]

Table 1. Continued.

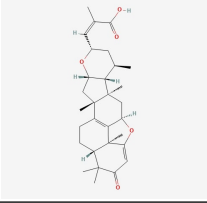
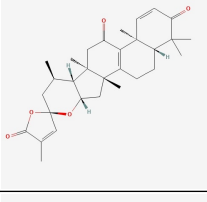
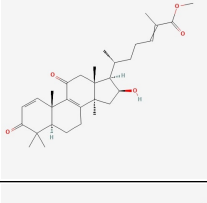
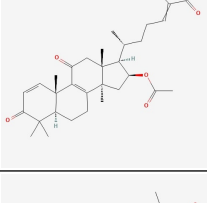
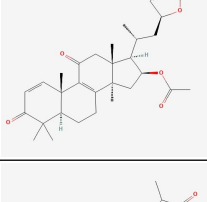
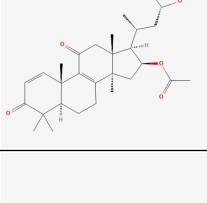
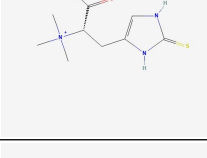
S.No.	Compound	Source	Structure	Reference
41	Lepiotaprocerin D	<i>Macrolepiota procera</i>		[24]
42	Lepiotaprocerin G	<i>Macrolepiota procera</i>		[24]
43	Lepiotaprocerin H	<i>Macrolepiota procera</i>		[24]
44	Lepiotaprocerin I	<i>Macrolepiota procera</i>		[24]
45	Lepiotaprocerin K	<i>Macrolepiota procera</i>		[24]
46	Lepiotaprocerin L	<i>Macrolepiota procera</i>		[24]
47	L-Ergothioneine	<i>Pleurotus ostreatus</i>		[24]
48	Peptidoglycan	<i>Pleurotus ostreatus</i>		[24]

Table 1. Continued.

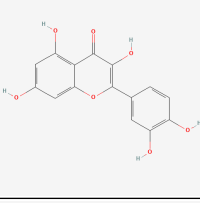
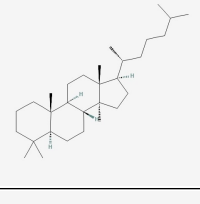
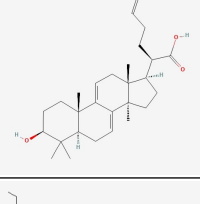
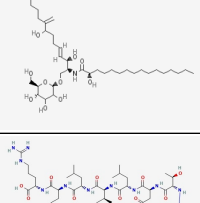
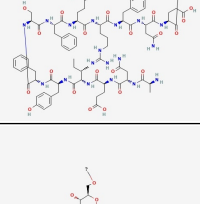
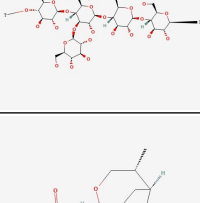
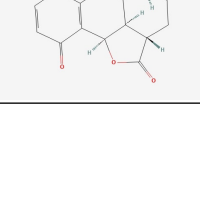
S.No.	Compound	Source	Structure	Reference
49	psilocybine	<i>Psilocybe semilanceata</i>		[24]
50	Queretin	<i>Pleurotus ostreatus</i>		[25]
51	Lanostane	<i>Wolfiporia cocos</i>		[25]
52	Dehydrotrametenolic acid	<i>Wolfiporia cocos</i>		[25]
53	Termitomycesphins	<i>Termitomyces albuminosus</i>		[25]
54	Lectin	<i>Xylaria hypoxylon</i>		[25]
55	Krestin	<i>Trametes versicolor</i>		[25]
56	Pleurotine	<i>Pleurotus griseus</i>		[25]

Table 1. Continued.

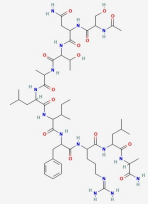
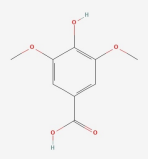
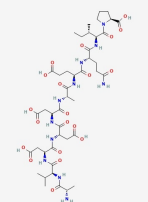
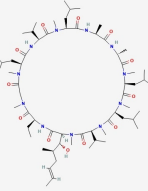
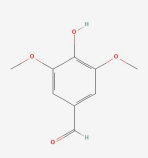
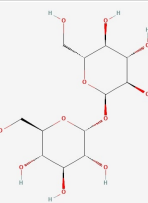
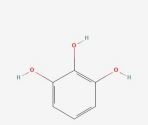
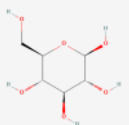
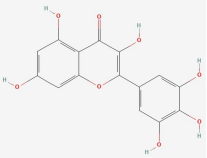
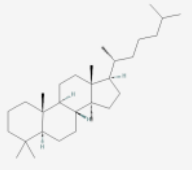
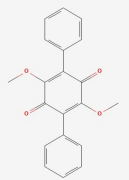
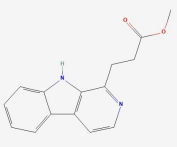
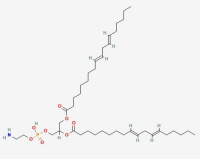
S.No.	Compound	Source	Structure	Reference
57	Ling Zhi-8	<i>Ganoderma lucidum</i>		[25]
58	Galactomannan	<i>Morchella esculenta</i>		[25]
59	Syringic acid	<i>Elaphomyces granulates</i>		[25]
60	Laccase	<i>Clitocybe maxima</i>		[25]
61	Ciclosporin	<i>Cordyceps sinensis</i>		[26]
62	Syringaldehyde	<i>Elaphomyces granulatus</i>		[26]
63	Trehalose	<i>Hypsizygus marmoreus</i>		[26]
64	Pyrogallol	<i>Cantharellus cibarius</i>		[26]

Table 1. Continued.

S.No.	Compound	Source	Structure	Reference
65	β -1,3-glucan	<i>Coprinus comatus</i>		[26]
66	Myricetin	<i>Craterellus cornucopiodes</i>		[26]
67	Lanostane	<i>Wolfiporia cocos</i>		[26]
68	Betulinan A	<i>Lenzites betulina</i>		[26]
69	Infracitin	<i>Cortinarius infractus</i>		[26]
70	Dilinoleoylphosphatidylethanolamine	<i>Hericium erinace</i>		[26]

All compounds administrated orally processed via the absorption, distribution, metabolism, and excretion process. Before considering any bioactive compound as a lead, it is imperative to check its ADME features so that any compound with inappropriate pharmacokinetics properties is filtered out [27,28]. The drug-like activity of the selected high-molecular-weight (HMW) and low-molecular-weight (LMW) edible mushroom compounds were categorized using the ADME properties shown in Table 2.

The physicochemical descriptors include molecular weight, molecular volume, H-bond donors, H-bond acceptors, and their position according to Lipinski's rule of five. Lipinski's rule of 5 is a rule of thumb to evaluate drug-

likeness; if a chemical compound contains specific pharmacological and biological properties, then properties would make it an active drug. The rule describes molecular properties important for a drug's pharmacokinetics in a living system, including ADME properties. All these pharmacokinetic parameters are within the acceptable range defined for human use, thereby indicating their potential as drug-like molecules. Lepiotaprocerin D had two rotatable bonds with a polar surface area (PSA) of 72.83 Å², whereas the number of rotatable bonds and PSA for peptidoglycan was 4 and 142.47, respectively.

Table 2. ADME/T properties of selected 5 bioactive compounds.

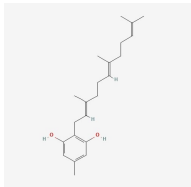
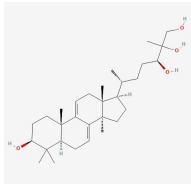
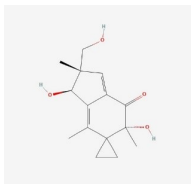
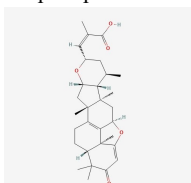
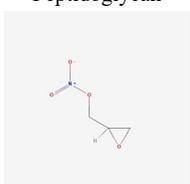
S.No.	Compound Name & Structure	Mol. Volume (m ³ /mol)	Mol. Weight (g/mol)	Rotatable Bonds	VdW PSA (Å ²)	RO5 Violation	HB Donors	HB Acceptors
	Grifolin							
1.		195.05	328.5	8	40.46	0	2	2
	Ganoderial							
2.		217.32	474.7	6	80.92	0	4	4
	Illudin S							
3.		121.00	264.3	1	77.76	0	3	4
	Lepiotaprocerin D							
4.		210.37	480.6	2	72.83	0	1	5
	Peptidoglycan							
5.		112.38	251.2	4	142.47	0	5	8

Table 3. The top five bioactive compounds exhibiting optimal binding affinity against BUB1B.

S. no.	Compound name	Binding energy	RMSD	Free energy (kcal/mol)	Internal energy (kcal/mol)
1.	Lepiotaprocerin D	-8.91	37.33	-2325.98	-8.18
2.	Peptidoglycan	-8.70	37.58	-2325.20	-7.40
3.	Grifolin	-8.14	35.37	-2325.00	-7.20
4.	Ganoderiol	-7.73	38.77	-2324.62	-6.82
5.	Illudin S	-7.08	35.19	-2324.86	-7.06

BUB1B, BUB1 mitotic checkpoint serine/threonine kinase B; RMSD, root-mean-square deviation.

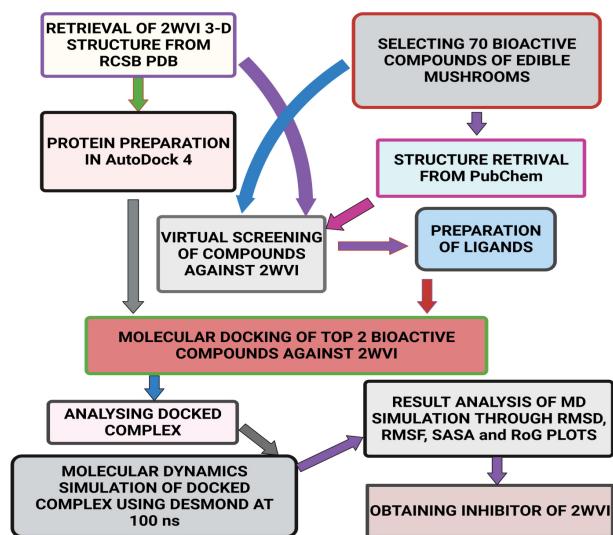


Fig. 2. Schematic representation of the methodology followed in the present study.

3.2 Molecular Interaction Analysis through Molecular Docking

The receptor BUB1B (PDB: 2WVI) was docked with the 70 compounds obtained from the literature survey. The active site of the BUB1B (2WVI) receptor consisted of Thr85, Tyr81, Gln58, Asp79, Tyr89, Ser96, Ser157, Tyr139, and Glu161 amino acid residues. The screening with AutoDock Vina found five compounds, i.e., grifolin, ganoderiol, illudin S, lepiotaprocerin D, and peptidoglycan as the most appropriate leads. These five compounds further docked against the BUB1B to obtain the best binding conformation and affinity. The docking showed well-formed binding of the identified lead compounds with one or more residues (amino acids) in the active site pocket of the 2WVI receptor shown in Fig. 3. Lepiotaprocerin D forms a hydrogen bond with 2WVI along with binding site residues of Ser157 and Glu161, and water bridges along Tyr139, Ser157, and Glu161. Peptidoglycan formed ionic interactions along Tyr81, hydrogen bond along Gln58, Tyr81, Thr85, and Tyr89, and water bridges along Gln58, Tyr81, and Tyr89 (Fig. 4).

The *in silico* molecular docking revealed that the newly identified compounds exhibit excellent binding energy towards the target receptor, as shown in Table 3.

3.3 Molecular Dynamic Simulation Analysis

Docking only provides a static view of the interaction between the receptor and compound in the active site of the protein receptor, it does not provide dynamic observation of the interaction. Molecular dynamic simulation offers to compute the binding atom movements with the time using Newton's motion. The molecular dynamic (MD) simulation was performed to determine the stability, confirmation, and intermolecular interaction of the top two ligand molecules (obtained from Autodock) with the 2WVI protein, as shown in Fig. 4a,b. The time-dependent modification of the complexes was calculated over 100 ns using the Desmond package. The MD simulation was performed under thermodynamics conditions (applied volume, density, pressure, and temperature). The complete system was annealed and equilibrated using ensembles. Moreover, the final production step was performed to investigate the structural modification of the complex.

3.4 Root-Mean-Square Deviation

Root-mean-square deviation (RMSD) is used to measure the deviation in the backbone of a protein from its initial structure conformation to its final position. This deviation, which is produced during MD simulation, determines the protein's stability relative to its conformation. A smaller deviation indicates a more stable protein structure. Ligand RMSD indicates the stability of the ligand with respect to the receptor (protein) and its respective binding pocket. The RMSD value for the ligand should be significantly lower than the protein RMSD because if this value is large, it is possible that the ligand may diffuse away from its initial binding pocket. From Fig. 5, it can be observed that for lepiotaprocerin D, the system equilibrated after 40 ns, after which the fluctuations were stable until 6 Å. The ligand was stable with respect to protein and confined to the binding pocket of the protein until approximately 48 ns, after which the ligand diffused away from the binding pocket owing to its RMSD value becoming larger than that of the receptor but again returning within the binding pocket after 52 ns. Similarly, for peptidoglycan, the system equilibrated after 10 ns, after which fluctuations stabilize for a short span, and then again, equilibration is obtained. We analyzed the conformer at specific times ($t = 10$ ns and $t = 55$ ns) and evaluated the conformation. Our analysis suggests that although the ligands were within the active site of the protein, there

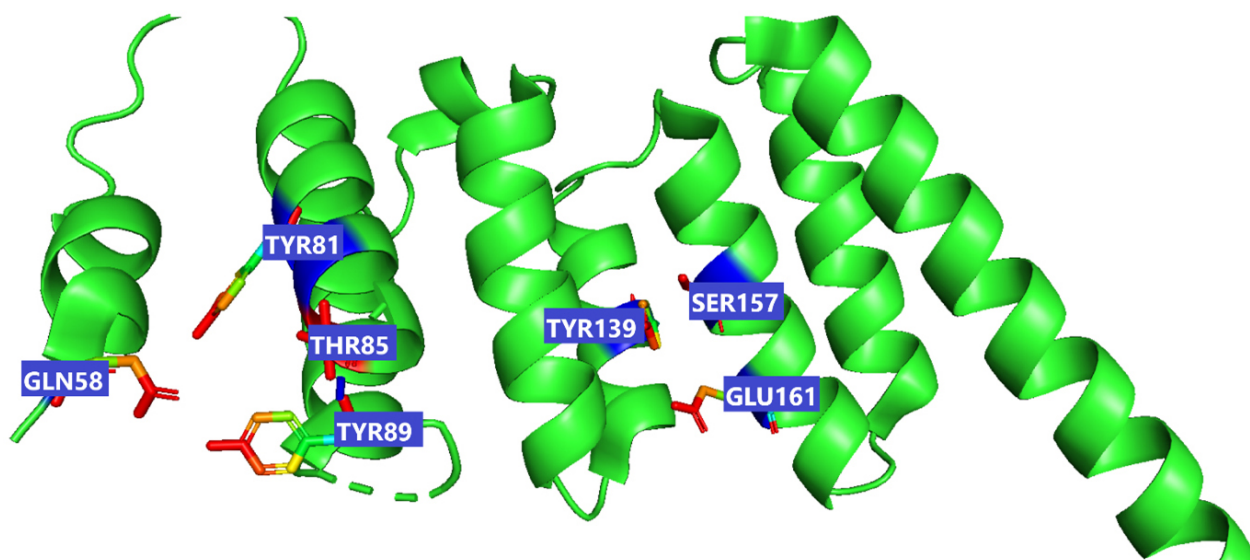


Fig. 3. This figure illustrate the active sites of 2WVI obtained from PyMol. The provided coordinates ($x_center = 0.4537$, $y_center = -24.6765$, $z_center = -12.2435$, $x_size = 60$, $y_size = 50$, $z_size = 70$) were used to generate the grid parameter file for the active site, which is located in chain-A of the protein spanning residues 72–165, illustrated in the figure which depicts the active site residues responsible for binding lepiotaprocerin D and peptidoglycan ligands. These residues include Gln58, Tyr81, Tyr89, Thr85, Tyr139, Ser157, and Glu161.

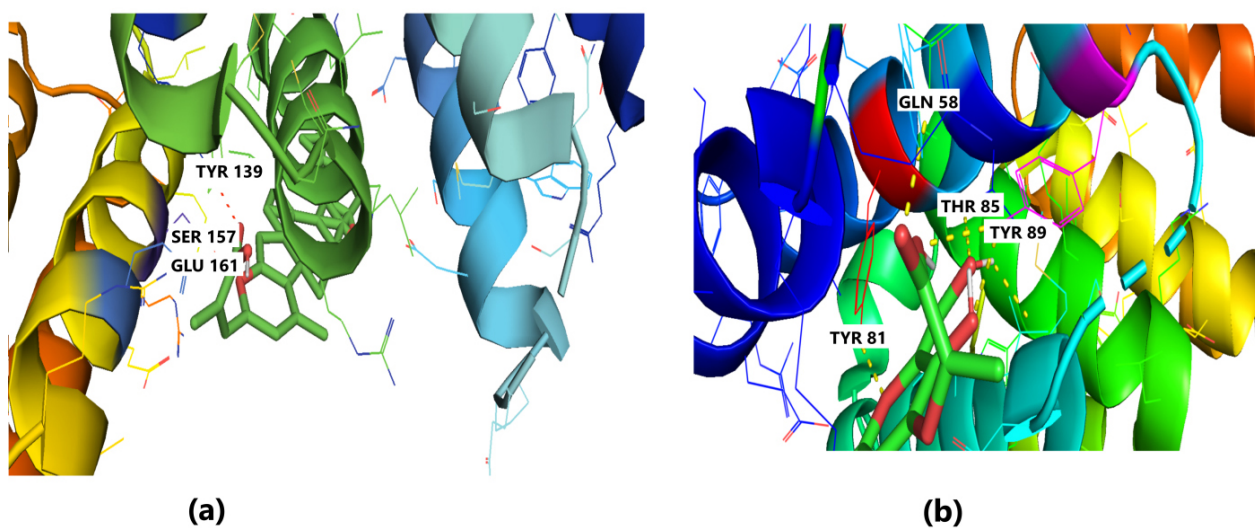


Fig. 4. Molecular Docking of 2WVI with the top two ligand molecules. (a) Lepiotaprocerin D forms a hydrogen bond with 2WVI and the binding site residues Ser157 and Glu161 and water bridges along Tyr139, Ser157, and Glu161. (b) Peptidoglycan formed ionic interactions along Tyr81, hydrogen bond along Gln58, Tyr81, Thr85, and Tyr89, and water bridges along Gln58, Tyr81, and Tyr89.

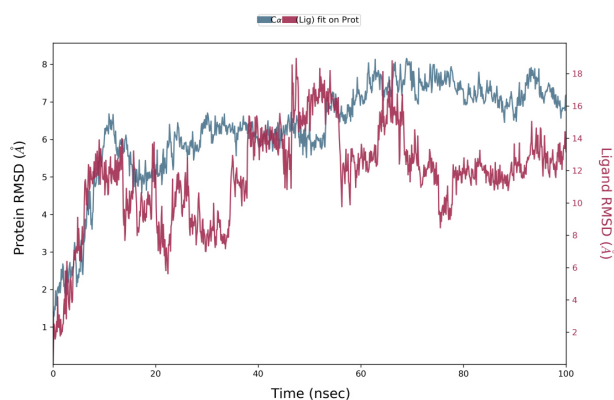
were some fluctuations between this interval which could explain the sudden rise of the amplitude of fluctuations.

3.5 Root-Mean-Square Fluctuation

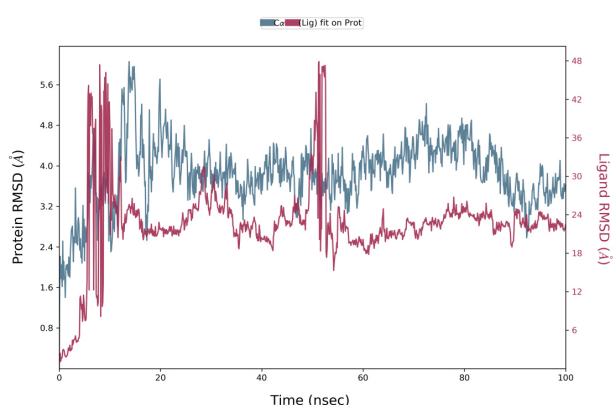
Root-mean-square fluctuation (RMSF) provides information about regions with higher flexibility levels. It measures the average deviation of atoms from their equilibrium positions over time, reflecting protein flexibility. Changes in the RMSF pattern can be correlated with protein

function or activity. Specifically, the flexibility in the region between 120–140 in the protein structure can affect its interaction with the ligand and thus impact the protein's activity. Understanding these dynamics may provide insight into the protein-ligand binding mechanism and inform the design of more effective drugs.

The RMSF plot peaks display the areas of maximum fluctuation of the protein. The $C\alpha$ backbone for peptidoglycan displayed a higher peak at residue number 30, which



(a)



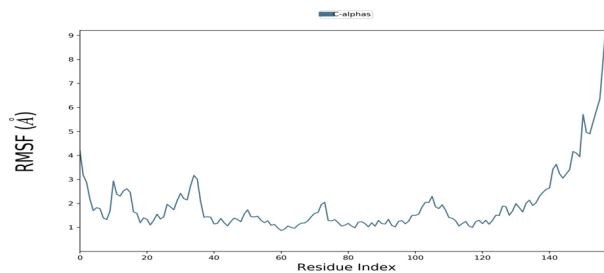
(b)

Fig. 5. Root-mean-square deviation (RMSD) plot. (a) RMSD plot for lepiotaprocerin D and 2WVI. X-axis on the left shows the RMSD for the 2WVI protein. The x-axis on the right shows the ligand (lepiotaprocerin D) stability. (b) The RMSD plot for peptidoglycan and 2WVI. X-axis on the left shows the RMSD for the protein (2WVI). The x-axis on the right shows the ligand (peptidoglycan) stability.

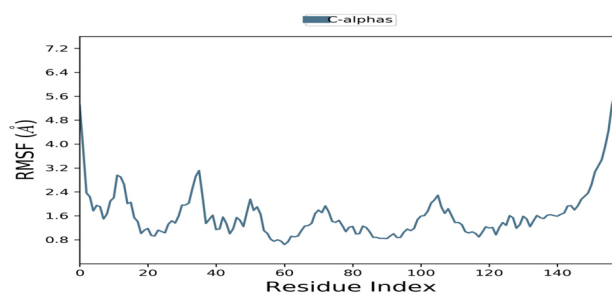
indicates more movement and also showed the most flexible residues around residue number 120 to 140 Fig. 6b. Similarly, in lepiotaprocerin D, the highest peak for the C α backbone, indicating more movement, was obtained at residue number 35. The most flexible residues were shown at residue numbers 40 to 80, shown in Fig. 6a.

3.6 Protein-Ligand Contacts

Protein-ligand interaction was observed throughout the simulation. There are four types of contact: hydrophobic, hydrogen bond, ionic, and water bridge. These intermolecular interactions play a vital role at an atomic level in predicting the binding mode of lepiotaprocerin D and peptidoglycan with the 2WVI receptor. Lepiotaprocerin D forms a hydrogen bond with 2WVI along with binding site residues of Ser157 and Glu161, and water bridges along



(a)



(b)

Fig. 6. Root-mean-square fluctuation (RMSF) plot. (a) RMSF plot of lepiotaprocerin D represents the flexibility level near residue number 30. (b) RMSF plot of peptidoglycan represents the flexibility level around residue numbers 120 and 140.

Tyr139, Ser157, and Glu161, shown in Fig. 4a. Peptidoglycan interacts with the BUB1B protein through ionic interactions with Tyr81, hydrogen bonding with Gln58, Tyr81, Thr85, and Tyr89, and water bridges with Gln58, Tyr81, and Tyr89. The hydrophobic interactions are relatively small in terms of interaction fraction as compared to those of lepiotaprocerin D, shown in Fig. 4b. Also, lepiotaprocerin D contained three binding site residues where interactions occurred more than 10% viz. Tyr139, Ser157, and Glu161. However, there were no interactions of more than 10% in peptidoglycan (Fig. 7a,b).

3.7 Radius of Gyration and Solvent Accessible Surface Area

The solvent-accessible surface area analysis and radius of gyration analysis were carried out to ascertain the level of compactness in the structure and the accessibility of the solvent to both lepiotaprocerin D and peptidoglycan. Solvent accessible surface area (SASA) analysis was performed using Desmond to investigate the binding affinity and potential inhibitory activity of two ligands (lepiotaprocerin D and peptidoglycan) with BUB1B. The SASA values of the protein-ligand complex were calculated for both bound and unbound forms. We focused on the SASA analysis to investigate the solvent-accessible surface area changes upon binding of each ligand to BUB1B. The SASA plots of the protein-ligand complex in both bound and unbound forms were generated to analyze the changes in the solvent-accessible surface area of the protein upon ligand

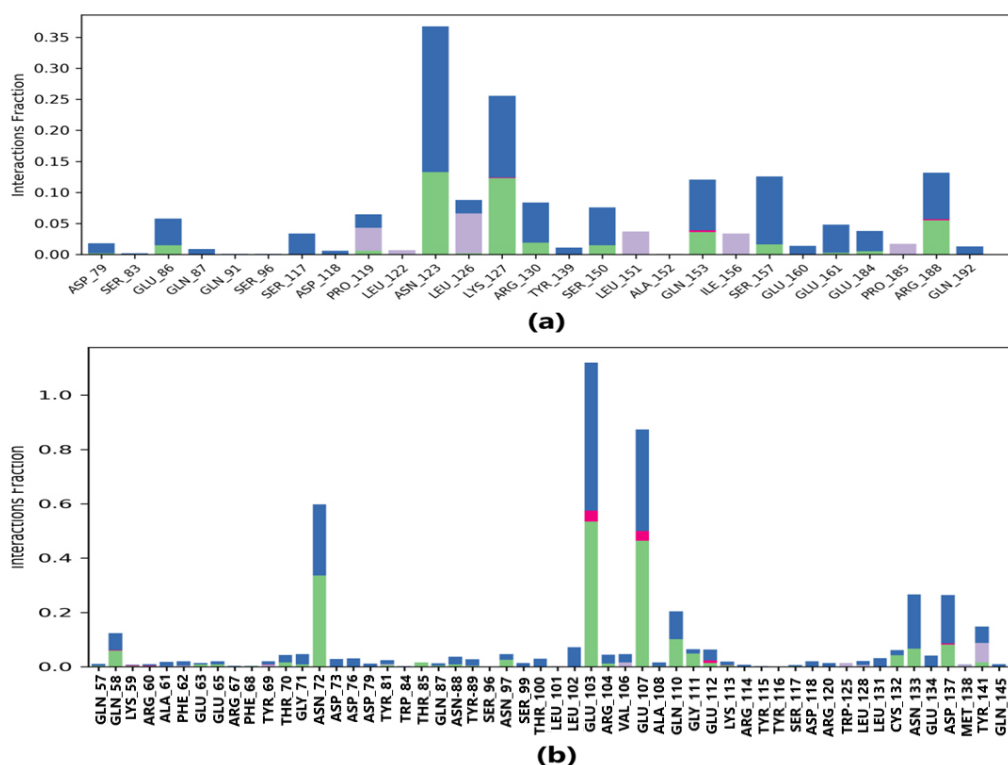


Fig. 7. Protein-ligand contacts. Blue indicates water bridges, green indicates H-bonds, grey indicates hydrophobic bonds, and pink indicates ionic bonding. (a) PL contacts showing amino acid residues corresponding to the interaction between 2WVI and lepiotaprocerin D. (b) PL contacts showing amino acid residues corresponding to the interaction between 2WVI and peptidoglycan.

binding. The radius of gyration of lepiotaprocerin D was observed from the figure as 19.8 Å (Fig. 8a), whereas peptidoglycan was 19.2 Å (Fig. 8b). The SASA plot also showed a higher value for lepiotaprocerin D as compared to peptidoglycan, shown in Fig. 9a,b.

4. Discussion

The present study focused on identifying naturally occurring edible mushroom compounds, such as *P. ostreatus*, with anticancer potential and the ability to inhibit BUB1B (2WVI). The leading cause of tumor progression is defective chromosomal segregation guarded by mitotic checkpoints [29–31]. This chromosomal instability causes aneuploidy which plays a vital role in tumorigenesis and cancer metastasis. The BUB1B protein, the primary component of the SAC, is responsible for corroborating proper chromosomal segregation [4,29–32]. Compared to normal cells, the over-expression of BUB1B in cancer cells regulates the tumorigenesis process. Hence, 2WVI is considered a potential therapeutic target for the treatment of cancers as its inhibition could reduce the process of aneuploidy, tumorigenesis and metastasis. The extract obtained from edible mushrooms, *P. ostreatus*, reportedly suppressed cell proliferation in breast and colon cancers through p53-dependent and p53-

independent pathways [10,31,32]. In this study, we predicted the drug-likeness properties based on the ADMET properties of 70 bioactive compounds extracted from edible mushrooms [33]. All 70 bioactive compounds qualified using Lipinski's rule of 5 (RO5). Lepiotaprocerin D, with a molecular weight of 480.60 daltons (<500), HBD count of 1 (<5), and HBA count of 5 (<10). Hydrogen bond acceptor (HBA) and hydrogen bond donor (HBD) counts were considered important parameters for the permeability and polarity of compounds. Lesser values of HBA and HBD indicated better efficacy and suitability of lepiotaprocerin D as a potential drug compared to peptidoglycan [18]. The molecular docking of 2WVI against these 70 compounds was carried out to obtain the best reasonable conformations for further studies. By screening and docking, five bioactive compounds, i.e., grifolin, gandriol, illudin S, lepiotaprocerin D, and peptidoglycan, were found to have a considerable binding affinity with 2WVI and therefore potential inhibitors of 2WVI. Two compounds, viz. lepiotaprocerin D and peptidoglycan, having the most negative affinities, were further selected for molecular dynamic study, for 100 ns simulation length, to obtain the dynamic behavior of atoms which provide information about structural changes, complex stability flexibility, and affinity at the atom and residue level. The RMSD analysis showed that lepiotapro-

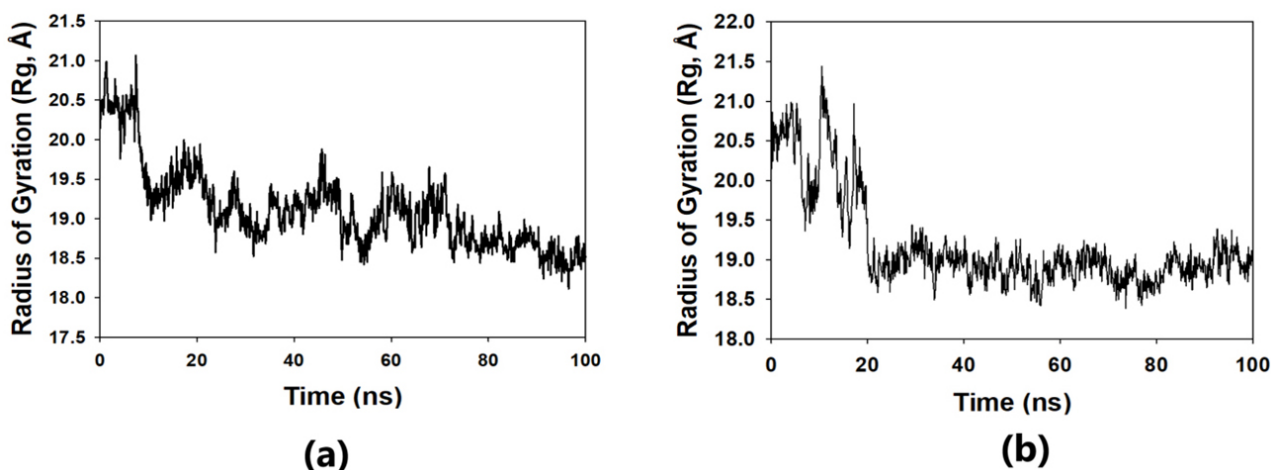


Fig. 8. Radius of gyration plot. (a) R_g plot for lepiotaprocerin D at 19.8 Å. (b) R_g plot for peptidoglycan at 19.2 Å. R_g , radius of gyration.

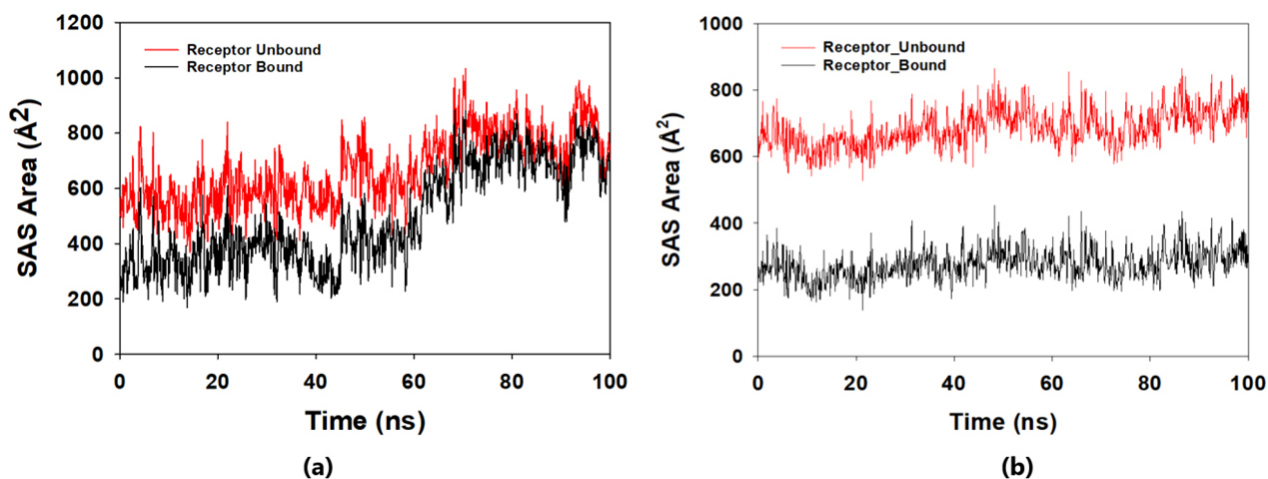


Fig. 9. Solvent accessible surface area (SASA) plot. The red fluctuation represents unbound receptor. The black fluctuation represents bound receptor. (a) The SASA plot shows a higher value for lepiotaprocerin D. (b) The SASA plot shows a lower value for peptidoglycan compared to lepiotaprocerin D.

cerin D was more stable than peptidoglycan as it has lower RMSD values than those of 2WVI until approximately 40 ns. The RMSF analysis, which was performed to measure fluctuation corresponding to each amino acid residue [34,35], indicated that lepiotaprocerin D has comparatively lower RMSF values of residues signifying less flexibility and more stability. Furthermore, the binding free energy for peptidoglycan (2325.20 kcal/mol) was weaker than that of lepiotaprocerin D (2325.98 kcal/mol). This was consistent with experimental results and proved the efficacy of lepiotaprocerin D as a potential drug candidate.

In this study, lepiotaprocerin D was bound with 2WVI along SER157, and this binding proposed this compound as the most suitable for inhibitor design. A novel discovery of this study was the formation of the hydrogen bond of ASN123 with lepiotaprocerin D which further strengthened the binding of 2WVI and lepiotaprocerin D as a potential in-

hibitor. Due to the highly helical nature of 2WVI in the case of lepiotaprocerin D, the binding between 2WVI and lepiotaprocerin D was found to be more stable. The radius of gyration that evaluates the compactness of protein structure was shown to decrease in lepiotaprocerin D, which gives an insight into the more stable conformation of the protein 2WVI. The decrease in the lepiotaprocerin D SASA supported our observation of the radius of gyration [36]. Hence, the molecular dynamic simulations parameters supported the efficacy of lepiotaprocerin D for the treatment of different cancers and could be used for the design of a suitable inhibitor that could reduce the effect of over-expressed 2WVI, thereby reducing tumorigenesis and metastasis of breast cancer and also the progression of glioblastoma multiforme (GBM) and hepatocellular carcinoma (HCC) [37].

The limitations of this study are that the above-discussed research work was carried out using an *in silico*

approach. Hence, the results will need to be validated using a wet lab approach to obtain the significance of the obtained results.

5. Conclusions

BUB1B is a primary element of the SAC. As over-expression of BUB1B is related to various cancers there is a need for suitable bioactive compounds to inhibit it with minimal toxic side effects. Thus, 70 bioactive compounds from edible mushrooms, which possess medicinal qualities and have proven anti-cancerous properties, have been screened against BUB1B. Structure-based *in-silico* approaches have been used, i.e., virtual screening, docking, and MD simulation. Two potential bioactive compounds lepiotaprocerin D and peptidoglycan, exhibited good drug-likeness and static affinity within the binding cavity of BUB1B through docking. Further dynamic studies using MD simulation (100 ns; RMSD, RMSF, radius of gyration (R_g), and SASA), revealed that lepiotaprocerin D has a considerably good binding affinity with BUB1B and forms an energetically favorable, stable, complex with BUB1B. Therefore, we determine lepiotaprocerin D as a novel inhibitor with high potential and a plausible drug candidate for BUB1B. As lepiotaprocerin D is derived from an edible mushroom, its use as an inhibitor against BUB1B may be safer and more effective.

Abbreviations

GBM, glioblastoma multiforme; HCC, hepatocellular carcinoma; ADMET, absorption, distribution, metabolism, excretion; SAC, spindle assembly checkpoint; R_g , radius of gyration; SASA, solvent accessible surface area; RMSD, root-mean-square deviation; RMSF, root-mean-square fluctuation; MD, molecular dynamic; HBD, hydrogen bond donor; HBA, hydrogen bond acceptor; HMW, high-molecular-weight; LMW, low-molecular-weight; RO5, Lipinski's rule of 5.

Availability of Data and Materials

Datasets used and/or analyzed for this study are available from the corresponding author upon appropriate request.

Author Contributions

All authors made substantial contributions to the conception and design of the work, as well as the acquisition, analysis, and interpretation of data. The specific contributions are as follows: Formal drafting, SNR, and SKS; Investigation and equal contribution to this work DM and AM; Project administration, MPS; Funding acquisition, EV. All authors contributed to editorial changes in the manuscript. All authors read and approved the final manuscript. All authors have participated sufficiently in the work to take public responsibility for appropriate portions of the content and

agreed to be accountable for all aspects of the work in ensuring that questions related to its accuracy or integrity.

Ethics Approval and Consent to Participate

Not applicable.

Acknowledgment

Not applicable.

Funding

This research received no external funding.

Conflict of Interest

The authors declare no conflict of interest. EV is serving as one of the Guest editors of this journal. We declare that EV had no involvement in the peer review of this article and has no access to information regarding its peer review. Full responsibility for the editorial process for this article was delegated to AA.

References

- [1] Wang S, Liu X, Yang M, Yuan D, Ye K, Qu X, *et al.* BUBs Are New Biomarkers of Promoting Tumorigenesis and Affecting Prognosis in Breast Cancer. *Disease Markers*. 2022; 2022: 2760432.
- [2] Lee E, Pain M, Wang H, Herman JA, Toledo CM, DeLuca JG, *et al.* Sensitivity to BUB1B Inhibition Defines an Alternative Classification of Glioblastoma. *Cancer Research*. 2017; 77: 5518–5529.
- [3] Bolanos-Garcia VM, Blundell TL. BUB1 and BUBR1: multifaceted kinases of the cell cycle. *Trends in Biochemical Sciences*. 2011; 36: 141–150.
- [4] Han JY, Han YK, Park GY, Kim SD, Lee CG. Bub1 is required for maintaining cancer stem cells in breast cancer cell lines. *Scientific Reports*. 2015; 5: 15993.
- [5] Jiao CY, Feng QC, Li CX, Wang D, Han S, Zhang YD, *et al.* BUB1B promotes extrahepatic cholangiocarcinoma progression via JNK/c-Jun pathways. *Cell Death & Disease*. 2021; 12: 63.
- [6] Weaver RL, Limzerwala JF, Naylor RM, Jegannathan KB, Baker DJ, van Deursen JM. BubR1 alterations that reinforce mitotic surveillance act against aneuploidy and cancer. *eLife*. 2016; 5: e16620.
- [7] Qiu J, Zhang S, Wang P, Wang H, Sha B, Peng H, *et al.* BUB1B promotes hepatocellular carcinoma progression via activation of the mTORC1 signaling pathway. *Cancer Medicine*. 2020; 9: 8159–8172.
- [8] Rajewska J, Bałasińska B. Biologically active compounds of edible mushrooms and their beneficial impact on health. *Postępy Higieny i Medycyny Doswiadczalnej*. 2004; 58: 352–357. (In Polish)
- [9] A Ajith T, K Janardhanan K. Indian medicinal mushrooms as a source of antioxidant and antitumor agents. *Journal of Clinical Biochemistry and Nutrition*. 2007; 40: 157–162.
- [10] Gu YH, Leonard J. *In vitro* effects on proliferation, apoptosis and colony inhibition in ER-dependent and ER-independent human breast cancer cells by selected mushroom species. *Oncology Reports*. 2006; 15: 417–423.
- [11] Bobek P, Ozdin L, Kuniak L. Antioxidative effect of oyster mushroom (*Pleurotus ostreatus*) in hypercholesterolemic rat. *Die Pharmazie*. 1995; 50: 441–442.

- [12] Sarangi I, Ghosh D, Bhutia SK, Mallick SK, Maiti TK. Antitumor and immunomodulating effects of *Pleurotus ostreatus* mycelia-derived proteoglycans. *International Immunopharmacology*. 2006; 6: 1287–1297.
- [13] Bobek P, Galbavý S. Hypocholesterolemic and antiatherogenic effect of oyster mushroom (*Pleurotus ostreatus*) in rabbits. *Die Nahrung*. 1999; 43: 339–342.
- [14] Jedinak A, Sliva D. *Pleurotus ostreatus* inhibits proliferation of human breast and colon cancer cells through p53-dependent as well as p53-independent pathway. *International Journal of Oncology*. 2008; 33: 1307–1313.
- [15] Tong H, Xia F, Feng K, Sun G, Gao X, Sun L, *et al.* Structural characterization and *in vitro* antitumor activity of a novel polysaccharide isolated from the fruiting bodies of *Pleurotus ostreatus*. *Bioresource Technology*. 2009; 100: 1682–1686.
- [16] Ebrahimi A, Atashi A, Soleimani M, Mashhadikhan M, Barahimi A, Kaviani S. Comparison of anticancer effect of *Pleurotus ostreatus* extract with doxorubicin hydrochloride alone and plus thermotherapy on erythroleukemia cell line. *Journal of Complementary & Integrative Medicine*. 2017; 15: 20160136.
- [17] Facchini JM, Alves EP, Aguilera C, Gern RMM, Silveira MLL, Wisbeck E, *et al.* Antitumor activity of *Pleurotus ostreatus* polysaccharide fractions on Ehrlich tumor and Sarcoma 180. *International Journal of Biological Macromolecules*. 2014; 68: 72–77.
- [18] Cao XY, Liu JL, Yang W, Hou X, Li QJ. Antitumor activity of polysaccharide extracted from *Pleurotus ostreatus* mycelia against gastric cancer *in vitro* and *in vivo*. *Molecular Medicine Reports*. 2015; 12: 2383–2389.
- [19] Katara P. Role of bioinformatics and pharmacogenomics in drug discovery and development process. *Network Modeling Analysis in Health Informatics and Bioinformatics*. 2013, 2: 225–230.
- [20] Kesharwani A, Chaurasia DK, Katara P. Repurposing of FDA approved drugs and their validation against potential drug targets for *Salmonella enterica* through molecular dynamics simulation. *Journal of Biomolecular Structure & Dynamics*. 2022; 40: 6255–6271.
- [21] Ma Q, Liu Y, Shang L, Yu J, Qu Q. The FOXM1/BUB1B signaling pathway is essential for the tumorigenicity and radioresistance of glioblastoma. *Oncology Reports*. 2017; 38: 3367–3375.
- [22] Trott O, Olson AJ. AutoDock Vina: improving the speed and accuracy of docking with a new scoring function, efficient optimization, and multithreading. *Journal of Computational Chemistry*. 2010; 31: 455–461.
- [23] Sánchez C. Bioactives from Mushroom and Their Application. In Puri M (ed.) *Food Bioactives* (pp. 23–57). Springer: Cham, Heidelberg. 2017.
- [24] Divya M, Aparna C, Mayank R, Singh MP. In-silico insights to identify the bioactive compounds of edible mushrooms as potential MMP9 inhibitor for Hepatitis-B. *Research Journal of Biotechnology*. 2021; 16: 2.
- [25] Manikandan K. Nutritional and medicinal values of mushrooms. *Mushrooms Cultivation, Marketing and Consumption*. 2011; 11–14.
- [26] Froufe HJC, Abreu RMV, Ferreira ICFR. Virtual screening of low molecular weight mushrooms compounds as potential Mdm2 inhibitors. *Journal of Enzyme Inhibition and Medicinal Chemistry*. 2013; 28: 569–575.
- [27] Morris GM, Huey R, Lindstrom W, Sanner MF, Belew RK, Goodsell DS, *et al.* AutoDock4 and AutoDockTools4: Automated docking with selective receptor flexibility. *Journal of Computational Chemistry*. 2009; 30: 2785–2791.
- [28] Guan L, Yang H, Cai Y, Sun L, Di P, Li W, *et al.* ADMET-score - a comprehensive scoring function for evaluation of chemical drug-likeness. *MedChemComm*. 2018; 10: 148–157.
- [29] Siemeister G, Mengel A, Fernández-Montalván AE, Bone W, Schröder J, Zitzmann-Kolbe S, *et al.* Inhibition of BUB1 Kinase by BAY 1816032 Sensitizes Tumor Cells toward Taxanes, ATR, and PARP Inhibitors *In Vitro* and *In Vivo*. *Clinical Cancer Research*. 2019; 25: 1404–1414.
- [30] Tang X, Guo M, Ding P, Deng Z, Ke M, Yuan Y, *et al.* BUB1B and circBUB1B_544aa aggravate multiple myeloma malignancy through evoking chromosomal instability. *Signal Transduction and Targeted Therapy*. 2021; 6: 361.
- [31] Lobanov MI, Bogatyreva NS, Galzitskaia OV. Radius of gyration is indicator of compactness of protein structure. *Molekuliarnaia Biologiia*. 2008; 42: 701–706.
- [32] Mishra D, Mishra A, Katara P, Singh MP. *In silico* identification of potential inhibitors of MPS1 from edible mushroom (*Pleurotus ostreatus*) to prevent aneuploidy and tumorigenesis. *Journal of Proteins and Proteomics*. 2022; 13: 175–185.
- [33] Bouback TA, Pokhrel S, Albesheri A, Aljohani AM, Samad A, Alam R, *et al.* Pharmacophore-Based Virtual Screening, Quantum Mechanics Calculations, and Molecular Dynamics Simulation Approaches Identified Potential Natural Antiviral Drug Candidates against MERS-CoV S1-NTD. *Molecules (Basel, Switzerland)*. 2021; 26: 4961.
- [34] Samad A, Ahammad F, Nain Z, Alam R, Imon RR, Hasan M, *et al.* Designing a multi-epitope vaccine against SARS-CoV-2: an immunoinformatics approach. *Journal of Biomolecular Structure & Dynamics*. 2022; 40: 14–30.
- [35] Alam R, Samad A, Ahammad F, Nur SM, Alsaiari AA, Imon RR, *et al.* *In silico* formulation of a next-generation multi-epitope vaccine for use as a prophylactic candidate against Crimean-Congo hemorrhagic fever. *BMC Medicine*. 2023; 21: 36.
- [36] Ramos M, Burgos N, Barnard A, Evans G, Preece J, Graz M, *et al.* *Agaricus bisporus* and its by-products as a source of valuable extracts and bioactive compounds. *Food Chemistry*. 2019; 292: 176–187.
- [37] Mishra D, Mishra A, Rai SN, Vamanu E, Singh MP. Identification of Prognostic Biomarkers for Suppressing Tumorigenesis and Metastasis of Hepatocellular Carcinoma through Transcriptome Analysis. *Diagnostics*. 2023; 13: 965.